A registered public-data reproducibility benchmark for the reported PKiKP detection of a Martian inner core

Artus Krohn-Grimberghe

Percivio Ltd.
Corresponding author: artus@percivio.com
ORCID: 0009-0001-4384-8306

Preprint statement. This manuscript is a non-peer-reviewed preprint submitted to EarthArXiv. It has not yet been submitted to a journal at the time of posting; submission to *Seismica* is planned.

Data and code availability. All inputs are public. The complete pipeline, registered criteria, and hash-pinned artifacts are available at https://github.com/Percivio-Ltd/mars-inner-core-benchmark and archived at https://doi.org/10.5281/zenodo.21762439.

A registered public-data reproducibility benchmark for the reported PKiKP detection of a Martian inner core

Artus Krohn-Grimberghe — Percivio Ltd.

Corresponding author: artus@percivio.com. ORCID: 0009-0001-4384-8306.

Abstract

Bi et al. (2025) infer a 600-km Martian solid inner core partly from a PKiKP vespagram peak at 604 ± 2 s after P and −6.5 ± 0.6 s/deg from stacked InSight marsquakes. We present a registered public-data reimplementation; success criteria, windows, and statistical rules were frozen before outcome inspection, and the headline lane uses the public MPS deglitch stage. We recover a local maximum inside the published target box (601.95 s, −6.67 s/deg), but it never wins: the registered argmax is a displaced ridge (663.8 s, −3.64 s/deg) at 1.21× the target-box power, and six single-event removals each hand the 23-event stack's argmax to a time-adjacent shallow-slowness branch. Composition–outcome association gives $p = 0.0039$ and 1.0×10^{-4} in two same-data designs. Distance scrambles exceed ridge power in 75.5% of realizations and target-box-maximum power in 48.0%. A same-path $\alpha = 0$ control exactly reproduces 4,600,000 cells; non-attested exploratory injections first win at $\alpha = 0.25$ in processed-trace pre-P-RMS units. The authors' raw-data deglitch method on the executable 19-event sub-stack preserves the qualitative disagreement and target-box subordination (box maximum cell-identical) while the global-argmax coordinate is deglitch-sensitive. This is reproducible non-agreement plus internal fragility, not a refutation; artifacts are released hash-pinned.

Non-technical summary

A recent high-profile study reported that Mars has a solid inner core, partly based on a faint seismic echo (PKiKP) found by stacking many marsquakes recorded by NASA's InSight lander. We rebuilt that analysis from scratch using only public data and code, and we wrote down all of our decision rules before looking at the results. Our reconstruction does find a secondary feature at the reported location — but the strongest feature in the search window is an unexplained one about a minute later, and whether that later feature stays on top depends on single marsquakes: remove any one of six specific quakes from the stack of 23 and the top spot shifts to a feature near the reported arrival time (though not with the reported apparent-velocity signature). This does not disprove the inner-core detection: a public Octave route to the authors' UCLA stage now exists, while our accepted headline lane remains MPS-only. It does show that the public-data version of the measurement is not yet robust, and it provides an openly verifiable benchmark that the community — including the original authors — can run and extend.

1. Introduction

The detection of core-transiting seismic phases from single-station planetary data is among the hardest measurements in seismology. Bi et al. (2025) report PKiKP and PKKP arrivals in stacked InSight data and infer a solid inner core of ~600 km radius for Mars. The claim rests on vespagram peaks recovered from low signal-to-noise stacks of order-20 events recorded by a single station, after event-specific deglitching, polarization filtering, alignment on direct-P picks, and slant stacking.

Results of this kind are, by construction, difficult for the community to check: the waveform data are public, but the processing pipeline is a sequence of outcome-sensitive choices (event selection, deglitching, polarization operator, normalization, alignment, stacking exponent, peak selection) whose interaction determines whether a marginal feature appears. Reproducibility work in this regime faces a specific epistemic trap: reimplementers have many degrees of freedom too, so an uncontrolled "failed to reproduce" is as weak as an uncontrolled detection.

We therefore built the reimplementation as a registered benchmark. All outcome-sensitive analytical choices — event set, windows, target boxes, tolerance rules, stacking parameters, bootstrap designs, statistical thresholds, and peak-selection rules — were frozen in a versioned specification before the affected outcomes were inspected, with deviations recorded on a registered amendment log stating why each change is not fitted to results. For the current claim-bearing replay, the repaired input audit binds the expected manifest before execution, retained products record their input identities, and the exercised missing/stale-provenance adverses fail closed. This evidence does not attest every historical execution. Positive and adverse controls accompany each claim-bearing step.

This paper reports what that benchmark finds: a reproducibly displaced argmax, a subordinate but supported local maximum inside the published-pair target box, and — the central result — a quantified single-event fragility of the displaced ridge's rank-1 status. We state at the outset what this is not: our pipeline is not the authors' pipeline, and agreement with the published coordinates was never a success criterion. A reproducible disagreement, honestly bounded, is the deliverable.

2. Data

All inputs are public and checksum-manifested: 2,693 path+SHA rows represent 2,393 distinct paths, with 300 duplicate-path rows carrying identical digests. The repaired current audit binds and verifies the expected manifest before the claim-bearing replay:

- **Waveforms.** InSight SEIS VBB (Lognonné et al., 2019) 20 sps BHU/BHV/BHW MiniSEED for 26 catalogued marsquakes (PDS `urn:nasa:pds:insight_seis` v3.0 via IRIS), cut around each event.
- **Catalog and picks.** MQS V14 event catalog (DOI 10.12686/a21): preferred origins, event metadata, and direct-P picks used for alignment.
- **Reference models.** The public AK model subset (DOI 10.18715/IPGP.2021.kpmqrnz8; Stähler et al., 2021) and the Khan et al. (2023) model ensemble (DOI 10.18715/IPGP.2023.llxn7e6d), used for TauP (Crotwell et al., 1999) travel-time context and provenance-tracked model comparisons.
- **Published pick tables.** The Bi et al. (2025) supplementary tables, archived with per-file SHA-256 and converted to CSV for the comparison surfaces.

The PKiKP stack uses the 23 events assigned `set=vespagram` by the registered event-set split; the other three (S1102a, S1153a, S1415a, at 73–88° distance) are registered `set=validation` events, processed through alignment and normalization but reserved from the stack. Stack support at the reported features is 23/23.

3. Methods

3.1 Pipeline

The chain is: deglitching → UVW→ZNE rotation → polarization filtering → alignment and cutting on MQS direct-P picks (common grid [−100, 2200) s relative to P) → normalization →

vespagram slant stacking → registered peak detection and comparison → bootstrap resampling → validation. The chain is implemented in Python on ObsPy (Beyreuther et al., 2010).

- **Deglitching** uses the public MPS/SEISglitch method (Scholz et al., 2020; pinned to an exact upstream commit, run in a pinned legacy environment for bit-stable behavior). For the UCLA half of the published two-method scheme, a public MATLAB archive exists (`UCLA_v4`); at the time the benchmark ran, no maintained executable route was available to this pipeline, so the UCLA stage was not reproducibly executed. The pipeline records the honest attestation `succeeded_mps_only` (26/26 events), records the strict two-method attestation `mps_ucla_verified` as failed, accepts the partial lane by design, and treats this as a first-class, visible limitation rather than an approximation to hide. A registered feasibility card (2026-08-01, dated addition) subsequently established that the archive is executable without MATLAB: it runs under GNU Octave with a two-line shim on a single used-path incompatibility, reproducing the package's own shipped reference fixtures to machine precision. A registered single-event equivalence card then compared the Octave route against the authors' shipped MATLAB reference on S0235b under a rule frozen before the run and classified the outcome DIVERGENT-MINOR: per-channel glitch counts 43/43, 34/34, and 36/37, port-noise ratios 0.04–0.09 (all within the 0.1 bound), with two unpaired detection neighborhoods and +10/+20-sample fit-window offsets (one to two samples on the 2-sps detection grid) — the published package's glitch selection is not platform-stable at the margin. The strict `mps_ucla_verified` attestation remains deliberately reserved, and every headline result in this paper is MPS-only. A registered production card (2026-08-02, dated addition) subsequently executed the UCLA stage end-to-end: the archive's shipped code crashes on four of the 26 events (empty-glitch-list indexing on two, a zero subscript at a detection edge, and a too-short segment fed to filtering), so a 22-event executable partition (19 stack + 3 validation events) was frozen a priori and the full benchmark chain was run twice over it — once with `UCLA_v4` deglitching the raw input directly (an explicit identity pre-stage records the terminal status `ucla_unverified`; no MPS processing is claimed) and once with the MPS lane restricted to the same partition, so the deglitch method is the single factor differing between lanes. Byte-identity controls anchored both lanes — the production UCLA product for S0235b equals the single-event census product, and the subset MPS product equals the accepted canonical product — and an adverse control confirmed that the excluded events are rejected mechanically by the lane's allow-list rather than discretionarily. The comparison itself is reported in § 5.5.

- **Polarization filtering** uses a public Montalbetti–Kanasewich-style principal-axis/DOP projection (after Montalbetti & Kanasewich, 1970; labeled as a public approximation; the authors' exact operator is not released), with a labeled principal-axis-projection ablation as an alternative operator.
- **Vespagrams** are fourth-root slant stacks (Muirhead & Datt, 1976) on envelope input at reference distance 29.0°, slowness −10…0 s/deg (100 steps), 20 s power window, minimum stack support 2. The registered primary lane is `paperfaith/envelope/A/montalbetti_kanasewich_1970/nth_root/20.0 s`.
- **Peak comparison** uses frozen target boxes from the published values: PKiKP 584–624 s × [−7.1, −5.9] s/deg (published 604 ± 2 s, −6.5 ± 0.6 s/deg); PKKP 1320–1360 s × [−8, −6] s/deg. Distance uncertainty is folded into the tolerance audit (a 2° distance uncertainty at ~7 s/deg is ~14 s of moveout, not a ±2 s coordinate tolerance).
- **Bootstrap.** Type I (event resampling), Type II (distance-stratified), and Type III (±10 s P-pick jitter) designs, N = 200, labeled `methods_robustness_200`: these quantify the robustness of our methods, and are not claimed to be equivalent to the published bootstrap.

3.2 Registration and governance

Seven success criteria were frozen in the specification, none of which require agreement with the published coordinates. Outcome-sensitive rules live on a dated, append-only amendment log; each amendment states why it is not outcome-fitted. Peak-selection for the leave-one-out analysis (§ 4.3) was frozen — including its branch boundary at 632.0 s — before execution, and when its positive control initially failed (the card's literal "full-grid" argmax rule found a grid-edge artifact), the repair was made by a registered pre-execution amendment adopting the production window-and-support rule, not by silently patching code. Every claim-bearing run carries a positive control (known-true reproduction) and an adverse control (deliberate corruption must fail closed); adverse failures stop the pipeline rather than degrade it. Supplementary Table S1 compacts the recorded outcomes of these controls for every claim-bearing surface, including four documented control weaknesses and their registered dispositions. The full benchmark was subjected to three independent model-assisted completion reviews; all confirmed the § A.4 criteria with zero P0 (invalidating) findings, with earlier-round P1 findings repaired and re-reviewed.

3.3 What is deliberately not claimed

Phase identity is never asserted for any feature; travel-time consistency with computed branches is reported as interpretive context only. Bootstrap outputs are methods-robustness statistics. The composition-association test (§ 4.3) is a same-data calibration, not an independent replication.

4. Results

4.1 The benchmark reproduces a displaced argmax

A retained accepted run (every configured stage succeeded, validation passed, and provenance enforcement requested; all 26 events deglitched `succeeded_mps_only`, with the strict `mps_ucla_verified` attestation failed and the MPS-only lane accepted by design) yields, in the registered primary lane: a supported PKiKP-window argmax (inclusive 550–700 s window, full −10…0 s/deg slowness grid, minimum support 2) at **663.80 s, −3.64 s/deg** (support 23/23) versus the published **604 s, −6.5 s/deg** — a displacement of **+59.8 s** in time and ≈ +2.9 s/deg in slowness (Fig. 1; Table 1). The peak-comparison table is SHA-256-identical under the declared run environment and repository root to the table produced three weeks earlier across an inventory change (`8df5f5c8…`). Cross-root LOO replay reproduced all argmax semantics but 0/24 NPZ container hashes because absolute paths are embedded; the reproducible object is therefore the path-neutral scientific semantics, not NPZ container bytes. The displaced ridge is configuration-stable under one argmax implementation: at the registered 20-s power window the envelope-variant maxima are 663.80 (A), 664.10 (B), and 664.85 s (C), and the separate 1-s power-window sweep places the analogous ridge at 662.05–662.80 s across variants A–C — neighboring cells on the same broad ridge, with the spread a power-window and normalization sensitivity, not a second independent reader.

Table 1 — registered-lane peak-table extract

Lane: paperfaith / envelope / A / montalbetti_kanasewich_1970 / nth_root / 20.0 s. Source: `results/tables/peak_comparison.csv` (SHA-256 `8df5f5c85473…`).

Phase	Feature	t (s)	s (s/deg)	Power	Δt vs row reference (s)	Exact tol.	Folded tol.	Broad-window rank	Bg. quantile
PKiKP	global	663.80	−3.64	0.9327	+59.80	False	False	1	0.7549
PKiKP	published target	601.95	−6.67	0.7736	−2.05	False	True	6938	0.7141
PKKP	peak 1	1235.35	−5.96	0.2777	−54.65	False	False	1	0.4784
PKKP	peak 2	1291.70	−4.75	0.2432	−49.30	False	False	2130	0.4411
PKKP	paper target	1341.00	−6.97	0.2143	+0.00	True	True	13395	0.3927

Row references for Δt: PKiKP rows use (604.00 s, −6.5 s/deg); PKKP peak 1 uses (1290.00 s, −8.0 s/deg); PKKP peak 2 and paper target use (1341.00 s, −7.0 s/deg).

Global-to-target-box power ratio: 1.2056 (recorded S3 statistic). PKKP mirror: rank 13395, background quantile 0.3927, within folded tolerance.

Table 1. Registered-lane peak-table extract: argmax vs target-box features for both phases, with ranks, background quantiles, power ratio, and tolerance flags.

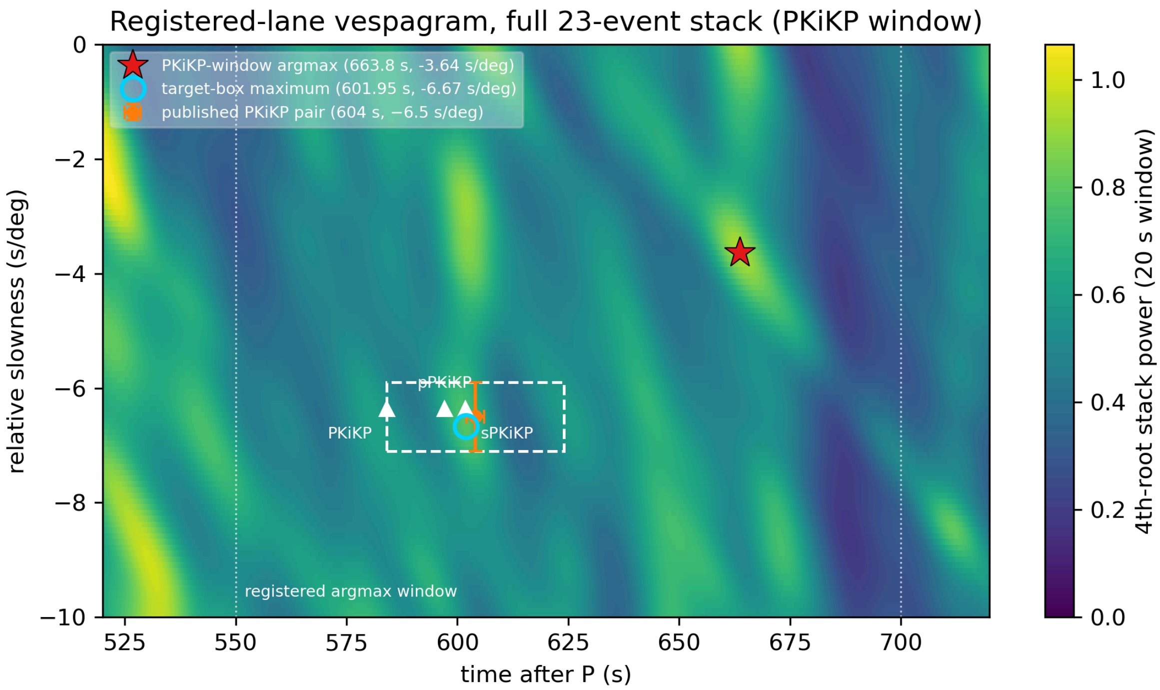

Figure 1. Registered-lane vespagram (23-event stack, 520–720 s view) with the displaced ridge argmax, the target-box maximum, the published pair and its uncertainties, the frozen target box, the registered 550–700 s argmax window, and the reference-model PKiKP-family overlay (PKiKP, pPKiKP, sPKiKP).

Inside the published-pair target box, the pipeline finds a supported, support-complete local maximum at **601.95 s, −6.67 s/deg** — within the uncertainty-folded tolerance of the published pair (though outside the raw ±2 s / ±0.6 s/deg box). A supported local maximum is therefore present inside the target box in the public reconstruction; it is just never the argmax.

4.2 How subordinate is the target-box feature?

Under the registered significance reading (rules frozen before inspection): the target-box maximum ranks **6,938th** among supported grid cells in the lane, sits at background quantile **0.714**, and carries stack power 0.774 against the displaced ridge's 0.933 — a power ratio of **1.21** in the ridge's favor (Table 1). The PKKP-side mirror statistic behaves analogously: a supported within-tolerance local maximum at 1341.0 s, −6.97 s/deg at rank 13,395 (background quantile 0.393), with the registered 20-s PKKP-window argmax elsewhere at approximately (1235.4 s, −5.96 s/deg).

We stress the reading discipline: (601.95 s, −6.67 s/deg) is the *maximum inside the published-pair target box*, not "the published PKiKP pair"; the published coordinates themselves are a box, not a cell.

Both statistics are calibrated by a registered same-data null (§ 5.4): under randomly sampled distance assignments from the registered permutation null that destroy moveout coherence, 75.5% of scrambled realizations of the same stack reach the displaced ridge's power and 48.0% reach the target-box maximum's.

4.3 The ridge's rank-1 status is six-events fragile

The central result. Three distinct features must be kept apart here: (i) the *target-box maximum* at 601.95 s, −6.67 s/deg; (ii) a *shallow 602-family branch* — time-adjacent to the published time but at shallow slowness; and (iii) the *displaced 662-family ridge* at 663.8 s, −3.64 s/deg.

Under the pre-registered leave-one-out design (branch boundary 632.0 s frozen in advance; deterministic 22-event restacks through the production loader and peak rule; byte-identical repeat control), the evaluated domain is 24 surfaces: the full stack plus 23 one-at-a-time removals. Removing any single one of **six** events — S0325a, S0474a, S0864a, S1012d, S1022a, S1039b — flips the supported PKiKP-window argmax from the displaced ridge to the shallow 602-family branch: the flips land at 602.0–606.4 s but at −3.43…0.0 s/deg, *outside* the target-box slowness range [−7.1, −5.9] (Fig. 2; Table 2). The target-box maximum itself never becomes the argmax in any removal. The flips are not marginal: exact shifts span 57.45–61.85 s, displayed to 0.1 s with decimal half values rounded up as 57.5–61.9 s. The other seventeen removals move the argmax by at most **0.95 s**. There is no intermediate case.

Table 2 — the six flipping events

Sources: `loo_table.csv` (LOO sweep) and `comp_assoc_reading.json` (max-T FWE composition test; Δ incl. = P(incl | 662-branch) − P(incl | early-branch), same-data calibration). FWE column lists the design(s) flagging the event: I = event resampling, II = distance-stratified, — = neither. Absolute shifts are rounded to 0.1 s with decimal half values rounded up.

Event	Distance (deg)	Held-out argmax t (s)	s (s/deg)	|Δt| (s)	FWE	Δ incl. (I)	Δ incl. (II)
S0325a	39.7	602.25	−3.43	61.6	—	+0.020	+0.149
S0474a	29.1	606.35	0.00	57.5	II	+0.164	+0.226
S0864a	28.7	601.95	−2.83	61.9	—	+0.141	+0.117
S1012d	38.3	602.15	−2.63	61.7	II	+0.206	+0.206
S1022a	30.7	602.20	−2.83	61.6	I+II	+0.218	+0.307
S1039b	30.4	602.05	−2.83	61.8	I+II	+0.267	+0.360

Table 2. The six flipping events: distance, flip landing coordinates (all at shallow slowness), |Δt|, per-design FWE status, and per-design Δ inclusion probability.

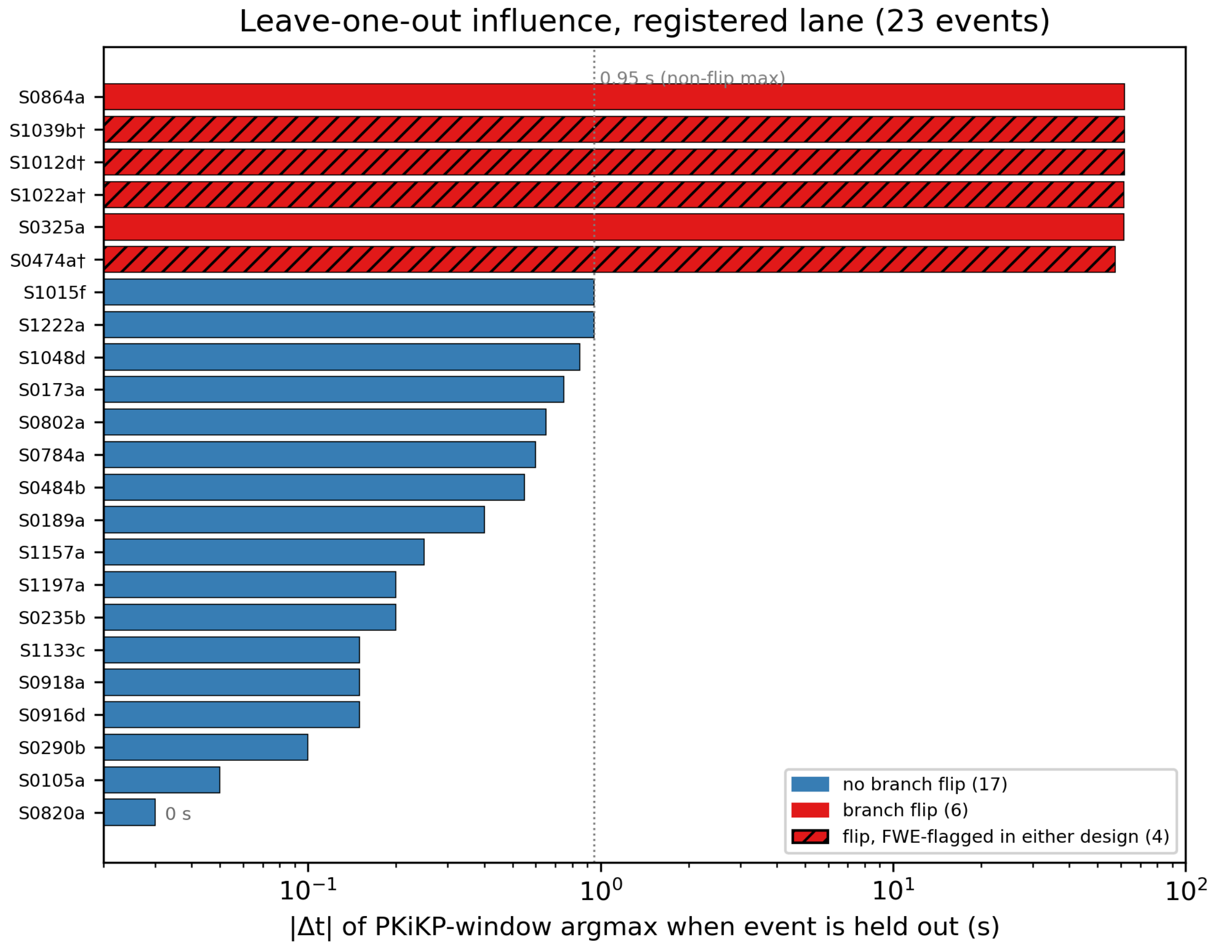

Figure 2. Leave-one-out sweep: $|\Delta t|$ of the supported PKiKP-window argmax per held-out event (log scale) — six removals flip it by 57.5–61.9 s, the other seventeen move it by $\leq$ 0.95 s; flips marked when FWE-flagged in either bootstrap design. All six flips land on the shallow-slowness 602-family branch, not on the target-box maximum.

Within those 24 surfaces, the displaced ridge is the argmax in the full stack and loses under each of the six corresponding single removals. Multi-removal interactions were not tested. What the sweep establishes is fragility of the *ridge's rank-1 status* against a time-adjacent shallow-slowness competitor; it does not show the target-box maximum winning under any removal. Four of the six flip events (S0474a, S1012d, S1022a, S1039b) are exactly the flip-set events flagged by the family-wise-error-controlled composition test below; two (S0325a, S0864a) were not flagged by the registered resampling diagnostics and were found only by the sweep.

Complementary composition evidence, all registered before reading:

- **Composition association.** Under label-permutation nulls that provably sever the association, the 602-vs-662 branch outcome is materially associated with event-set composition in both bootstrap designs (Type I max-T $p = 0.0039$; Type II $p = 1.0 \times 10^{-4}$). By design, the FWE-significant events are: Type I — S1039b and S1022a (inclusion favors the 662 branch); Type II — additionally S0474a and S1012d positive, and S0820a and S0484b negative (inclusion favors the early branch); see Table 2. Registered honesty clauses: this is a same-data calibration, and — because mean selected distance is a deterministic function of event composition within the fixed event table — distance and composition effects are not separately identifiable from these products.
- **Occupancy bimodality.** Type I bootstrap occupancy for PKiKP is bimodal: 602–603 s regions dominate at the 50% and 70% thresholds while the 664 s region dominates at 85% — both occupancy families occur under the registered conditional resampling (Fig. 3).
- **Design comparison.** The 662-branch fractions are Type I 0.635 (95% CI [0.566, 0.699]) and Type II 0.550 ([0.481, 0.617]). Their Wilson intervals overlap descriptively; no equivalence margin or paired comparison was registered, so no equivalence conclusion follows (Fig. 3).
- **PKKP contrast.** The instability is feature-specific, not pipeline-generic: on the PKKP side the registered occupancy-cell argmax is stable-early under both bootstrap designs — Type I and Type II agree at all three occupancy thresholds (largest $|\Delta t| = 1.65$ s, largest $|\Delta s| = 0.20$ s/deg, well inside the frozen $|\Delta t| \leq 5$ s, $|\Delta s| \leq 0.5$ s/deg concordance rule), with every reading nearest the early ~1236 s, −6.1 s/deg feature and no PKiKP-style branch competition between thresholds or designs.

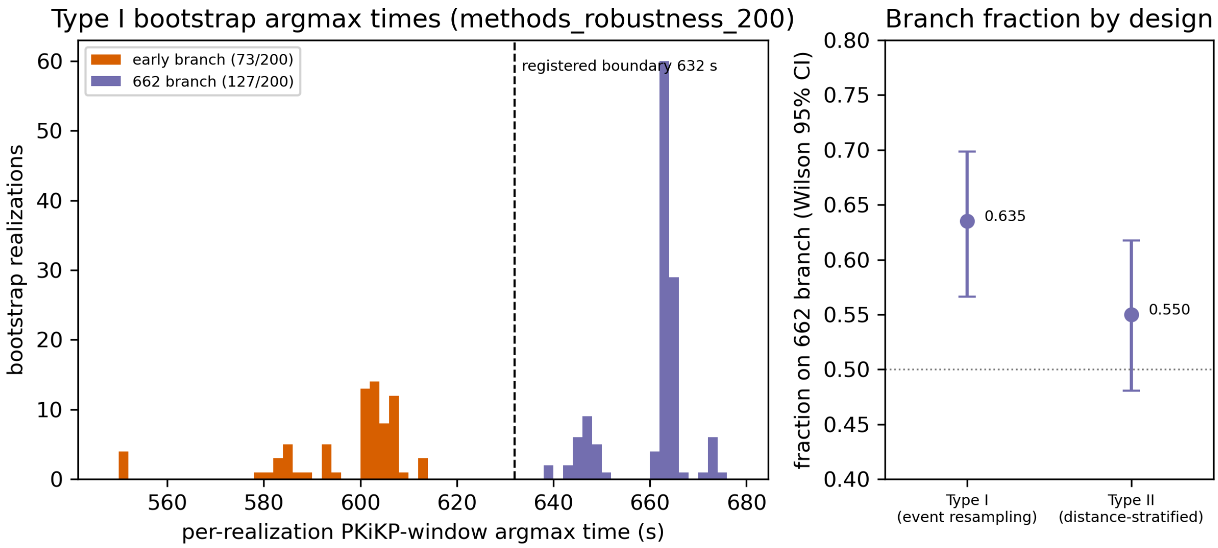

Figure 3. Type I bootstrap argmax-time bimodality (N = 200, registered 632.0 s branch boundary) and 662-branch fractions with Wilson 95% CIs for both bootstrap designs.

4.4 What does *not* explain the displacement

- **Alignment error.** The registered ±10 s P-pick jitter audit changes the PKiKP weighted occupancy centroid by 5.05 s, broadens its nonzero support 31.24×, and yields zero target-box global winners in these 200 realizations (Fig. 4b). The demonstrated-power 60 s exploratory lane shifts the centroid by 27.88 s. These centroid statistics are not distributional upper bounds or a feature-tracking exclusion test.
- **Polarization operator.** Swapping the M-K-style operator for the labeled principal-axis ablation leaves the target-box maximum non-global under both operators; the subordinate within-tolerance local maximum at the target-box coordinates is operator-robust. The *identity* of the envelope-A winner, however, is operator-sensitive: at the registered 20-s window the principal-axis winner is a shallow-slowness time-adjacent feature at 603.25 s, −3.54 s/deg (601.90 s, −3.54 s/deg in the 1-s power-window sweep) — note: not the target-box maximum, whose slowness is −6.67. The operator swap thus removes most of the *time* displacement in envelope A while leaving the slowness mismatch and the target-box subordination in place; the 662 s ridge survives the swap in envelope variants B and C (Fig. 4a).
- **Kinematics.** At the registered geometry (29.0°, 33 km depth), the published pair and the target box are kinematically consistent with the reference-model PKiKP family (model slowness ≈

−6.36 s/deg). Zero branches in the registered reference-model query are consistent with either competing feature (the registered 1-s comparison points F2 = 662.05 s, −3.43 s/deg and F1 = 601.9 s, −3.54 s/deg). On the PKKP side, zero branches in the query match the observed features or the first published reference; the second published reference (1341.0 s, −7.0 s/deg) is consistent with PKIKKIKP. The registered query, in other words, finds kinematically consistent branches at the published coordinates and none at the features that outcompete them — an asymmetry of model consistency, not a prediction of detectability.

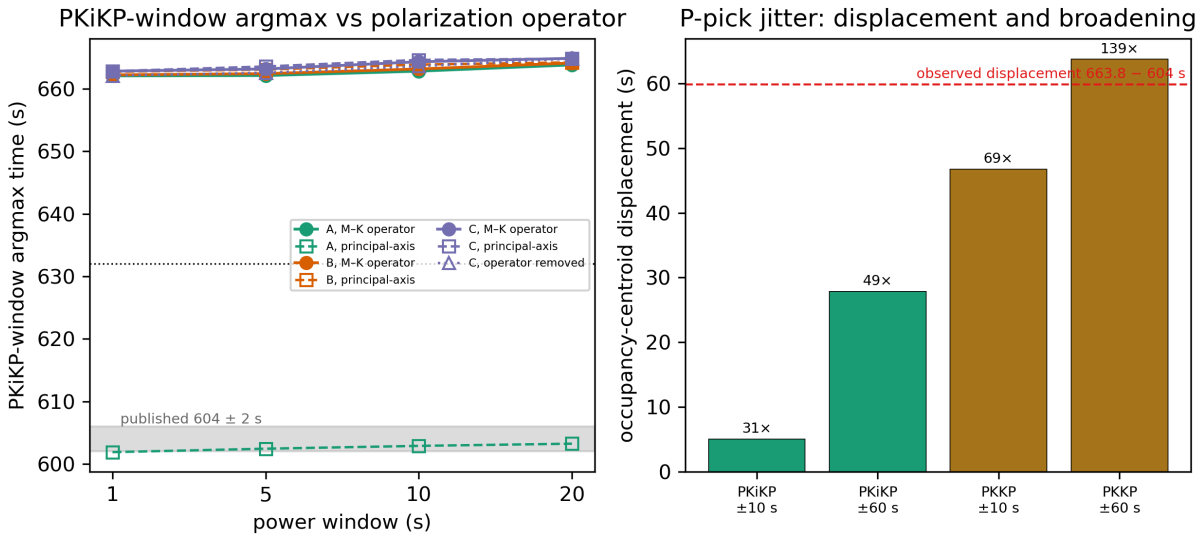

Figure 4. (a) PKiKP argmax time per envelope variant × polarization operator × power window; (b) jitter-audit centroid displacements and broadening ratios against the observed 59.8 s displacement.

4.5 Chain integrity

The current claim-bearing replay is guarded by a repository-resident identity verifier binds every evidence locator to its digest (a transplanted digest fails closed); vespagram payloads verify lane identity against path identity before any merge; the model stage re-queries the generated travel-time model and requires registered P/PKiKP times within 0.01 s; and the repaired current non-from-scratch replay begins with a verify-only audit bound to the expected manifest (the three source ZIP archives are digest-pinned nonresident by a registered amendment, with byte-verified custody copies in object storage). Adverse controls for each guard are demonstrated in the test suite (criterion-scoped run: 1,271 passed / 1 skipped / 0 failed). These current controls do not assert unconditional equivalence between standalone-validator and full-orchestrator assurance in every execution context or historical run.

5. Discussion

5.1 The deflationary reading, taken seriously

A referee should hold, and we hold, the deflationary reading: our pipeline is not the authors' pipeline. The deglitch lane is MPS-only where the original applied a second, in-house UCLA-lineage step; the polarization operator is a public reconstruction; the alignment and normalization are ours; the bootstrap is a methods-robustness instrument. "The public reconstruction disagrees" could in principle mean "the public approximation is insufficient," not "the claim is fragile." Two findings survive that reading, because they are internal to our own pipeline:

1. **The invariant.** Across both polarization operators, all envelope variants, and a byte-stable rerun across environments, the target-box maximum is never the argmax. The operators disagree about what wins; they agree about what loses.
2. **The single-removal domain.** Even granting every approximation, within this one fixed pipeline the displaced ridge's rank-1 status trades against a time-adjacent shallow-slowness branch on the removal of any one of six specific events. Across the evaluated full stack plus 23 one-at-a-time removals, two of those events were not flagged by the registered resampling diagnostics. Multi-removal interactions were not tested; the demonstrated fragility is confined to this 24-surface analysis.

5.2 Model-conditioned peak selection

The kinematic asymmetry of § 4.4 suggests the generalizable methodological point: in low-SNR single-station stacks, peak selection conditioned on a model prediction will find a peak where the model says to look — the target-box feature is a supported local maximum within folded tolerance — while a stronger unexplained feature can sit nearby, invisible to a search that never leaves the box. Vespagram detections of this kind should routinely report (i) the global-versus-box rank and power ratio of the candidate, and (ii) a single-event leave-one-out sweep of the global argmax. Both are nearly free to compute and either would have surfaced the fragility reported here. An independent re-analysis has since instantiated the same structural concern in model space, by scanning the conditioning model itself (§ 5.6).

5.3 Calibration on independently constrained ground: the lunar-analog blind test

The methodological concern of § 5.2 is not hypothetical: the identical machinery has been calibrated once, blind, on a body whose deep interior is independently constrained — not gospel ground truth (the lunar estimates are themselves stacking-derived, a caveat its pre-registration records), but independent of the machinery under test. In a companion experiment (2026-07-06) we ported the source-array vespagram pipeline 1:1 to Apollo lunar long-period data — six of the seven modules byte-identical to the audited Mars implementation used here, the seventh differing in import mechanics only — and asked, under criteria frozen before any waveform contact (pre-registration SHA-256 `ab5f8034…`), whether it recovers the lunar core, whose radius carries independent estimates near 330–380 km (Weber et al., 2011; Garcia et al., 2011). The data were 228 quality-passing event-windowed traces from Apollo stations 12/14/15/16 (network XA), with events and per-station P arrivals taken from the Nakamura catalogue and the Nunn et al. (2020) compiled-arrival supplement; declared adaptations were confined to the data reality (principally long-period vertical only, no polarization filter, Lanczos resampling to 20 Hz, and a lunar −100… +1200 s cut window; the full declared list is in the archived report and pre-registration).

The pre-registration froze two detection grades so that the test could be rigged in neither direction. G1 ("paper-grade": $|\Delta T| \leq 25$ s, $|\Delta p| \leq 1.2$ s/deg, σ_T ≤ 10 s, σ_p ≤ 1.0 s/deg, occupancy ≥ 0.50, Type-III concordance) mirrors the precision the published Mars analysis reports; G2 ("replication-grade": $|\Delta T| \leq 50$ s, $|\Delta p| \leq 2.0$ s/deg, σ_T ≤ 50 s, σ_p ≤ 1.5 s/deg, occupancy ≥ 0.45) mirrors what our own Mars rerun actually achieves at the 85% occupancy threshold (σ_T = 43.0 s PKiKP, 49.3 s PKKP; `results/tables/bootstrap_picks.csv`). Held only to G1, the lunar test would fail a standard the Mars reproduction itself does not meet; held only to G2, it would pass trivially.

The pre-registered verdict was METHOD-FRAGILE at both grades. At G1 the method detected nothing on the real Moon (0 of 3 primary deep-moonquake configurations) while phase-randomized noise still "detected" a lunar core in 15% of realizations and station-swapped geometry in 33% — synthetic noise outperformed the actual Moon at the claimed precision. At G2 the method detected core reflections everywhere: real data 3/3, and distance-scrambled data 75/75, phase-randomized noise 72/75, station-swapped geometry 6/6, and 16 of 24 arbitrary decoy windows. The implied core radii of the surviving detections scatter from 100 to 470 km and disagree between stations far beyond the pre-registered consistency tolerance.

For the present benchmark this calibration closes a loop the Mars data cannot close by themselves. At replication-grade tightness, box-localized occupancy peaks arise unconditionally — in scrambled data and pure noise, at false-alarm rates near one — so whatever evidential weight such peaks carry must come entirely from the tightness of the reported uncertainties. That tightness is precisely the property the public reconstruction does not reproduce: the G2 grade above is anchored to our own rerun's σ_T. Cheap matched nulls — event-scramble and decoy windows — are the natural extension of the § 5.2 recommendations, and on the Moon they were the entire difference between an apparent detection and a demonstrable false alarm. Their Mars-side counterparts are reported in § 5.4.

The calibration has its own limits, recorded in its archived report. Apollo long-period data are a harder stacking target than InSight VBB data (intense scattering coda, 10-bit resolution, peaked instrument response), and the primary trace counts (11–16) sit below the Mars set's 23. Fragility on the Moon therefore does not prove the Mars detections false; what it demonstrates is that the method's internal consistency checks — bootstrap occupancy, multi-configuration presence — cannot by themselves distinguish true from false arrivals at these noise conditions and trace counts, and that null behavior must be characterized per dataset. One geometric caveat cuts in the method's favor: deep-moonquake sources compress the core-reflection slowness discriminant to ≈ −1 s/deg, intrinsically harder than the Mars PKiKP geometry (≈ −6.5 s/deg) — though surface-source impact configurations (≈ −3.4 s/deg) showed the same detect-everything pattern at G2.

The citable record is the archived report, the frozen pre-registration with its dated amendments, and the criteria/target/radius code, all in repository custody; the bulk run products of the 2026-07-06 campaign were not retained, and neither were the port's retrieval, preprocessing, and stacking runners. The protocol is therefore reconstructable in principle from the pre-registration and public Apollo data, but the exact experiment is not regenerable from retained custody alone. It predates this paper's registration regime and is cited as a dated companion experiment, not folded into this paper's provenance-enforced chain.

5.4 Same-data calibration of the detection machinery

The lunar calibration closed with an obligation rather than a conclusion: null behavior must be characterized per dataset (§ 5.3), and the dataset that matters here is the Mars stack itself. We therefore ran the § 5.2 recommendations on the benchmark's own data as three registered calibration cards — an event-scramble null (the Mars-side counterpart of the lunar N1 null), a synthetic injection ladder, and a decoy-box family statistic — each with statistics, thresholds, seeds, ladders, controls, and stop conditions frozen in a registered card text before that card executed, with dated, outcome-neutral amendments, and with memos, adjudications, control outcomes, and per-artifact hashes in repository custody. All three are same-data calibrations in the § 3.3 sense: they measure how the frozen detection criteria behave on this event set and noise field — when moveout coherence is destroyed, when a known coherent arrival is added, and when the target box is displaced across the surface. None re-measures propagation physics; none can prove the published detection true or false.

Event-scramble null. The null permutes the 23 catalogued epicentral distances across the stacked events (N = 200 seeded permutations; the identity assignment is excluded and carried separately), leaving traces, alignment masks, and envelopes untouched: moveout coherence is destroyed while the envelope population the stack integrates is preserved. The realization stack is the production stack — the runner imports the repository stacking and peak-detection code, and the identity permutation reproduces the canonical argmax and target-box cells with exact float equality, on stack grids array-identical to the canonical chain's. The regenerated canonical lane is line-identical to the production peak table (SHA-256 `8df5f5c8`…), an effect control confirms that permuted distances change the stack grid massively, and a repeated realization is byte-identical (Table S1e). All 200 realizations completed with no errors and no NaN statistics.

Against the frozen thresholds — 0.9327, the canonical ridge power, and 0.7736, the real target-box maximum — the null is not rare but modal: **151 of 200** scrambled realizations produce a supported

PKiKP-window argmax at or above the ridge power — a false-alarm rate of 0.755 (exceedance p = 152/201 = 0.756) — and **96 of 200** produce a target-box maximum at or above the real one (false-alarm rate 0.480; p = 97/201 = 0.483). The real ridge sits near the 24th percentile of its own scramble null — the null median, 0.979, exceeds it — and the real target-box maximum sits at the null median (0.767). (The fourth-root stack's power normalization permits null powers above unity — null maxima 1.333 and 1.076 — and thresholds were applied exactly as frozen, with no rescaling.)

Under the frozen criteria, then, supported argmax powers at or above the ridge threshold occur in 151/200 scrambles and target-box maxima at or above their real threshold occur in 96/200, under randomly sampled distance assignments from the registered permutation null. No separate occupancy statistic was computed. The registered honesty clause bounds the reading. This is a same-data calibration: the null destroys moveout coherence while keeping the envelopes, so it calibrates the machinery's false-alarm behavior on this noise field, not event-set propagation physics; it is conditional on the observed distance multiset; and event selection, alignment jitter, and renormalization are covered by the separate registered bootstrap lanes (§ 3.1). It proves no detection false; it calibrates the detection criteria themselves. With it, the matched null the lunar experiment showed to be decisive (§ 5.3, N1 firing 75/75 at replication grade) exists for the Mars data: the displaced 663.8-s ridge and the target-box maximum are both statistically unremarkable against the scramble null (Fig. 5) — the false-alarm-side complement of the leave-one-out fragility of § 4.3.

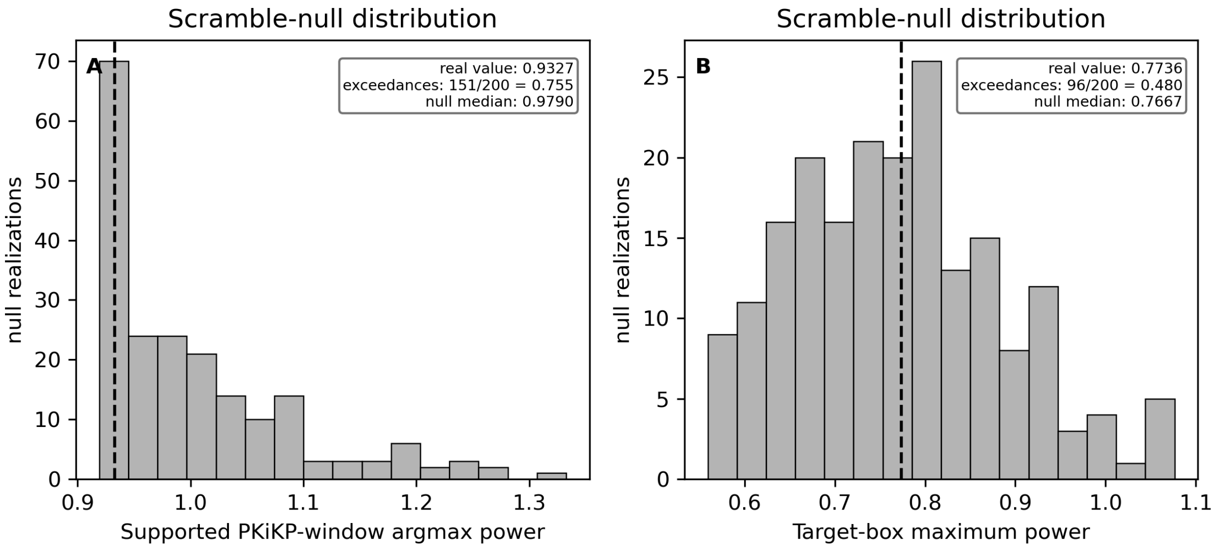

Figure 5. Scramble-null distributions (§ 5.4): supported PKiKP-window argmax powers (panel A) and target-box maximum powers (panel B) across the 200 null realizations, real values marked, recorded exceedance counts (151/200 = 0.755; 96/200 = 0.480) and null medians annotated.

Injection ladder. The scramble null calibrates false alarms; the injection ladder calibrates sensitivity — could this stack have seen a published-coordinate arrival, and at what amplitude does one out-compete the displaced ridge? Into each event's aligned, band-passed, polarization-filtered trace we injected a synthetic arrival at the published pair — an impulse at t_i = 604 + (−6.5)(Δ_i − 29°), band-limited by the chain's own 0.2–0.8 Hz zero-phase filter call — with peak amplitude α times that trace's pre-P (−60 to −10 s) noise RMS; α is a per-trace, pre-normalization SNR scale on the processed traces, and the registered ladder is α ∈ {0, 0.25, 0.5, 1, 2, 4, 8}. Everything downstream is the chain's own machinery (normalization, envelope, stacking, peak detection). The α = 0 lane reproduces the canonical cell field-for-field under full provenance enforcement; the injection convention is proven rather than assumed — the production shift formula recovers the injected time as 604.0 ± 0.051 s for 23/23 stacked traces in every lane — and repeated lanes are byte-identical. The injected lanes are exploratory by necessity (an injection invalidates the alignment-stage provenance hash by construction, and is recorded as such rather than masked). A subsequent same-path α = 0 control produced zero differing cells of 4,600,000, field-identical argmax and support, and unchanged α*_argmax = α*_power = 0.25 (`history/20260803_alpha0_samepath_control/`

`CONTROL.md`). Nonzero injected lanes remain exploratory and outside full provenance attestation; their mechanical claim rests on that enforced $\alpha = 0$ control and the determinism controls (Table S1e).

The measured flip is floor-limited (Table 3): $\boldsymbol{\alpha^*} = \mathbf{0.25}$, the smallest registered nonzero rung, under both frozen outcome definitions (argmax-in-box, and target-box power at or above the ridge's 0.9327). At $\alpha = 0.25$ the global supported argmax moves from the displaced ridge into the published target box, at (602.95 s, −6.46 s/deg) with power 1.248 against the ridge's 0.933, and it stays in the box at every larger rung. The true flip point therefore lies somewhere in (0, 0.25] and is not further resolved: no smaller rungs were registered, and none were added after the outcome was seen. Per the card's outcome-neutral framing, two readings follow. As sensitivity: the chain detects a coherent arrival at the published coordinates at ≤ 0.25× pre-P RMS amplitude, so the non-detection at $\alpha = 0$ is not explained by the machinery being too insensitive — provided a real arrival were as moveout-coherent as the synthetic one. As margin: the observed ridge's global dominance over the published-coordinate family is worth less than 0.25 in the registered processed-trace pre-P-RMS amplitude unit at the published coordinates — the amplitude-domain expression of the same fragility that § 4.3 measured in composition. The unresolved ideal-coherent crossing in (0, 0.25], rather than the tested 0.25 rung itself, is the quantity that would lower-bound the amplitude required by a less-coherent real arrival under this premise.

Table 3 — injection-recovery ladder

Source: `history/20260801_inject_recov/recovery_table.csv` (SHA-256 `0b7a66a46e3f`…).

alpha	Global argmax (time s, slowness s/deg, power, support)	Argmax in target box	Target-box max power	Target-box max time (s)
0	(663.80, −3.64, 0.9327, 23)	no	0.7736	601.95
0.25	(602.95, −6.46, 1.2483, 23)	yes	1.2483	602.95
0.5	(603.30, −6.46, 1.6204, 23)	yes	1.6204	603.30
1	(603.50, −6.46, 2.1772, 23)	yes	2.1772	603.50
2	(603.65, −6.46, 3.0591, 23)	yes	3.0591	603.65
4	(603.80, −6.46, 4.6325, 23)	yes	4.6325	603.80
8	(603.90, −6.46, 7.5507, 23)	yes	7.5507	603.90

a) alpha = 0 is the canonical enforced lane; injected lanes (alpha > 0) are exploratory by necessity (injection invalidates the alignment-stage provenance hash by construction).

b) the alpha = 8 literal positive control FAILED on the time axis (603.90 s, two 0.05-s cells from 604.0) and is adjudicated a control-tolerance design flaw; it is not quotable as a passed literal control (draft section 5.4; Table S1e).

Table 3. Injection-recovery ladder (§ 5.4): per registered rung $\alpha \in \{0, 0.25, 0.5, 1, 2, 4, 8\}$, the global argmax (time, slowness, power, support), in-target-box flag, and target-box maximum; footnotes fix the $\alpha = 0$ canonical-lane standing and the $\alpha = 8$ failed literal control.

One frozen control of this card failed, and is disclosed rather than repaired. The $\alpha = 8$ positive control required the recovered argmax to land within one grid cell of (604, −6.5); the observed argmax, (603.90 s, −6.46 s/deg), is within one slowness cell but 0.10 s — two 0.05-s time cells — early. The registered tripwire ran to the letter: the convention was re-verified exact, the rerun was byte-identical and failed identically, and the run stopped and reported rather than coding around the wording. Adjudication recorded the failure as a control-tolerance design flaw, not a convention or pipeline defect. The discriminating evidence: across the tested ladder the argmax times 602.95, 603.30, 603.50, 603.65, 603.80, and 603.90 s move toward 604.0 from the pre-existing in-box background maximum at 601.95 s. This is consistent with additive background peak-pulling under envelope smoothing at finite α, but the stage-isolation evidence does not uniquely establish that mechanism; a genuine convention error would displace the peak by tens of seconds, flip the recovered moveout sign, or collapse the 23-fold support, and would not converge. The α = 8 lane is therefore not quoted here as a passed literal control; the convention claim rests on the numeric shift-recovery check above.

The design bounds the reading in the machinery's favor. The injection is ideally coherent — exact −6.5 s/deg moveout at exact catalog distances, an identical wavelet in every trace, exact P-alignment — whereas a real arrival carries pick error, distance uncertainty, and waveform variability, all of which dilute coherent gain: α* from this design is a lower bound on the amplitude a real arrival would need. And α is a machine-level SNR scale on the processed, polarization-weighted traces, not a statement about raw ground motion.

Decoy-box family statistic. A third card asked the family-wise question latent in § 4.2: what fraction of target-box-sized (40 s × 1.2 s/deg) decoy boxes, slid across the frozen sweep span (box centers 250–2100 s, full slowness range), contains a maximum at least as high as the real target-box maximum? The box reader validated exactly, reproducing four independently recorded anchors — the canonical argmax cell, the target-box maximum 0.7736, the ridge-cell box 0.9327, and a PKKP mirror threshold 0.2143 recorded before the sweep — but the card's frozen adverse control failed: a box confined to the pre-P segment ([−90, −50] s × [−7.1, −5.9] s/deg), required to stay below 0.7736 on the premise that the pre-P surface is quiet, returned a supported maximum of **49.37**, independently re-derived from the stack file outside the reader. The run stopped, as registered.

Because the reader is proven correct, the failure is a data property of the canonical stacking surface — and that property, not any family fraction, is this card's finding. The variant-A supported-power surface carries an early-time trace-edge/normalization artifact ramp: 19 of 26 variant-A envelopes — the 23 stack traces plus 3 validation traces — carry onset transients 5–355× the target-window scale immediately after their valid-data onsets — trace-start/mask-edge energy amplified by the variant-A normalization — and these survive the minimum-support-2 mask with supported stacked power up to 1395 in the pre-P segment. The early sweep is not monotone: the 2.397 in-sweep box maximum at center 280 s exceeds the 1.8 reported over 150–250 s. Band-resolved, 100% of decoy boxes with centers in 250–400 s exceed both PKiKP thresholds, against 0% at 800–1600 s, with a small late trace-edge rise. The family fractions the card froze were computed but are confounded by this demonstrated ramp, and are therefore not accepted as false-alarm-style rates (they remain recorded, with the per-box tables, in the card's history record). The confirmatory family-rate lane on this surface is closed: the band-resolved outcomes have been seen, so any restricted-domain variant would be outcome-exposed and could only be exploratory, and a confirmatory family statistic would require a fresh registration whose null design excludes edge transients by per-event valid-data onset — designed, and honestly labeled as designed, after this mechanism finding. For the present benchmark the ramp is an additional reason the uncertainty-folded standing of the target-box maximum (§ 4.2) should not be over-read, and a documented instance of the control discipline doing its designed job: the adverse control stopped a confounded statistic before it entered this paper.

Taken together, the accepted calibrations bracket the detection machinery on the same data that produced § 4. On the false-alarm side, destroying moveout coherence leaves the PKiKP-window peak statistics essentially unchanged: ridge-level argmax power arises in 75.5% of scrambled realizations, and target-box maxima reach the real target-box power in 48.0%. These are the two computed power exceedance rates, not an occupancy statistic. On the sensitivity side, an ideally coherent published-coordinate arrival at one quarter of the per-trace pre-P noise RMS out-competes the displaced ridge. The ridge of § 4.1 is therefore simultaneously statistically unremarkable against its own scramble null, six-events fragile in composition (§ 4.3), and globally dominant by a margin worth less than 0.25× pre-P RMS of coherent target-coordinate energy; symmetrically, the target-box maximum's within-tolerance standing (§ 4.2) is a property that nearly half of the scrambled stacks reproduce, on a surface that additionally carries a demonstrated early-time artifact ramp. None of this proves the published detection false: these are same-data calibrations of a public reconstruction, and the deflationary reading of § 5.1

stands. What they establish is benchmark-internal and quantitative: on this surface, under these frozen criteria, neither the ridge-power nor target-box-maximum-power threshold discriminates moveout-coherent structure from moveout-incoherent alternatives, so the evidential weight of a detection must come from properties these nulls do not already reproduce — on the Moon that property was the tightness of the reported uncertainties (§ 5.3), and it is precisely the property the public reconstruction does not recover.

A fourth registered card executed the same frozen chain across the two published 23-event selections and their 21-event intersection. Because it answers a question about the relation to the independent re-analysis rather than about the machinery, its result — the headline structure is selection-invariant — is reported there (§ 5.6).

The triptych's Earth end executed as a registered single-station port of the frozen machinery to known-truth data: 33 usable vertical-component traces (from 40 selected events, M 6.2–7.8, 25.4–35.0°) at the quiet GSN borehole station ANMO, aligned on ak135-predicted P from catalog hypocenters, with three target phases (PcP primary, PKiKP secondary, ScS plausibility boundary), twelve decoy windows, a 25-realization event-scramble null, and two frozen grades mirroring the lunar pair — paper-grade G1 and deliberately lenient replication-grade G2 (run record `history/20260801_earth_ctrl/`). One registered control did not survive contact with the data: the pilot alignment gate (envelope argmax within ±10 s of predicted P) failed on the pilot trace — argmax at +29.25 s, the search-window edge, despite an envelope SNR of 66× the pre-P median — and the gate statistic was then replaced by an onset criterion under which the same trace passes. That replacement is a post-hoc criteria change outside the preregistration's frozen repair rule, which permitted fixing the alignment convention only; under the strict frozen reading the registered remedy for a pilot failure was to stop. The production run and everything reported below therefore carries exploratory, deviation-flagged standing, and is reported under that flag rather than not at all.

Under the frozen grading, the ported machinery did not recover the known phases: PcP is undetected at both grades — as are PKiKP and ScS — while the same-machinery nulls stay quiet (per-phase false-alarm rates 0.000–0.250, all below the frozen 1/3 quiet-null criterion), so the preregistered verdict is NOT-RECOVERED at both grades; at the replication grade the same stack also certifies two wrong-place decoy windows (Table S1f). No directional interpretation of the fitted-versus-predicted time offsets is drawn; the one initially offered did not survive countersign review and is retired in the run record. The triptych thus closes with both known-truth ends down: the lunar port returned METHOD-FRAGILE on hard data (§ 5.3), and the Earth port fails to recover PcP on easy data — large, well-located events on a quiet station — under its preregistered criteria. Neither known-truth exercise demonstrates that this machinery recovers known core phases under frozen criteria, which bears directly on the evidential weight a same-machinery detection on unknown-truth Mars data can carry, independent of the same-data nulls above.

5.5 Limitations

The MPS-only deglitch lane is the largest fidelity gap and is prominently attested in every product. The registered feasibility and single-event equivalence cards (§ 3.1, dated additions) established an executable public route to `UCLA_v4` and its DIVERGENT-MINOR standing against the authors' shipped reference, and a registered production card (2026-08-02, dated addition; § 3.1) then executed the follow-up those cards left open — a production UCLA-stage pass and its effect on the benchmark surfaces. The executable-partition result preserves the qualitative PKiKP disagreement and subordination of the published-target maximum under UCLA-on-raw provenance, but not the global-argmax coordinate itself. On the a-priori frozen 19-event sub-stack, with the deglitch method the single factor differing between lanes, the three registered readout surfaces compare same-cell as:

Registered surface	UCLA-on-raw (19-event stack)	MPS (19-event stack)	Accepted MPS (23-event stack, context)
PKiKP global argmax	576.15 s, −10.0 s/deg, power 0.9003	662.85 s, 0.0 s/deg, power 1.0140	663.80 s, −3.64 s/deg, power 0.9327
PKiKP published-box maximum	584.00 s, −7.07 s/deg, power 0.7547	584.00 s, −7.07 s/deg, power 0.7356	601.95 s, −6.67 s/deg, power 0.7736
PKKP endpoint	1341.25 s, −6.97 s/deg, power 0.3049	1340.95 s, −6.97 s/deg, power 0.2422	1341.00 s, −6.97 s/deg, power 0.2143

The published-box maximum lands in the identical native-grid cell under both deglitch methods (powers 2.6% apart); the PKKP endpoint is same-slowness and 0.30 s near-concordant, with a 25.9% relative power difference disclosed because no robustness tolerance was registered for that surface. The qualitative PKiKP disagreement persists: the UCLA lane's global maximum (power 0.9003) remains distinct from and stronger than its published-target row (power 0.7547), so the published-target maximum stays subordinate under UCLA provenance as well. The global-argmax coordinate, by contrast, is deglitch-sensitive — the UCLA lane selects a previously unobserved domain-edge argmax location (576.15 s, −10.0 s/deg), beyond the two branch families the leave-one-out control documents (§ 4.3) — so the argmax is branch-fragile to both event removal and deglitch method and is not a stable readout surface. The 23-to-19-event comparison also attributes the box-maximum displacement (601.95 ⟶ 584.00 s) to the event set rather than the deglitch method, since both deglitch lanes agree exactly at 19 events. Three bounds on the comparison: the UCLA lane's terminal status is `ucla_unverified` (the strict `mps_ucla_verified` attestation remains reserved; § 3.1); the comparison runs on the 19-event sub-stack rather than the full 23-event stack; and the persistence statement is qualitative — coordinate-level robustness holds only where stated cell-exactly above. N = 200 bootstrap realizations bound the resolution of occupancy statistics. The composition-association p-values are same-data calibrations, and distance and composition effects are not separately identifiable within the fixed event table. The operator-ablation table was originally recorded at `current_provenance_status=not_required`; a registered provenance-enforced rerun of the identical chain subsequently reproduced all 240 rows with exactly identical coordinates, every row at `current_provenance_status=current`, and a byte-flip adverse control failing closed — the ablation numbers used here carry full provenance standing. TauP context uses public reference models in a bounded registered query, not the authors' preferred interior models. Nothing here addresses the PKKP-side detection with the same depth as the PKiKP side.

5.6 Relation to the published claim and to independent re-analysis

Our result is a reproducible non-agreement plus internal fragility under a registered public reconstruction. It is not a refutation, and the original detection may survive exact-pipeline scrutiny.

If it does, this benchmark still stands as a public, runnable robustness benchmark for the claim — and the released, hash-pinned pipeline gives the original authors a concrete, runnable surface against which to demonstrate exactly which non-public step makes the difference.

While this work was in preparation, Visser, Munch, Khan, Frost, and Giardini (2026) — a team including InSight mission scientists — posted an independent re-analysis of the same event family. They compute linear-stack vespagrams together with an F-vespagram coherence statistic while varying the assumed inner-core radius of the conditioning model between 50 and 650 km, and report coherent, in-window candidates for multiple radii — 200–300 km and 500–600 km for PKiKP (with beam amplitudes for the 200- and 300-km models exceeding those of the 600-km model) and 100–600 km for PKIKKIKP — concluding that the data provide no definitive evidence for an inner core. Their diagnosis and ours are independent and complementary forms of non-uniqueness: their model-conditioned radius scan shows that a search conditioned on a model prediction finds candidates for many assumed radii (the § 5.2 concern instantiated in model space), while our registered reconstruction shows that at the published radius the published coordinates are not the dominant feature of the search surface, and that the dominant feature's rank-1 status is itself six-events fragile (§ 4.1–§ 4.3). The two studies share no code and differ in stacking method, filter band, and normalization, yet converge on the same conclusion: the reported phase attribution is not yet robust.

Two reproducibility-specific observations follow. First, their preprocessing (deglitched waveforms, Butterworth band-pass, Montalbetti–Kanasewich polarization filtering) sits in the same public-methods family as our reconstruction, which independently supports that this family is what the published description specifies. Second, their stack uses 23 events described as those considered by Bi et al. (2025), but the event list in their supplement differs from the frozen 23-event stack set declared in the Bi et al. supplementary tables (archived here with hash-pinned provenance): it omits S0105a and S0189a and includes S0409d and S0809a, two events that do not appear in the archived published event tables.

Rather than leaving the selection difference as a caveat, we executed the registered chain on Visser-ID 23 under registered MarsQuake metadata and on the 21-event intersection of the two selections (registered as a cross-selection card after their posting, with the two added events passed through the same gated deglitch-and-rotation lane). Membership was isolated by design; 17 of the 21 shared rows differ in quality and/or distance fields between the source tables. The headline structure is selection-invariant: in all three selections the global supported argmax is the displaced ridge in the same slowness cell at 663.80–663.95 s (rank 1), already fixed by the 21 shared events, while the published-coordinate box maximum stays subordinate throughout and sinks further under their selection (rank 6,938 canonical → 15,809 intersection → 25,172 Visser selection). This invariance is a non-monotone interaction, not a common-six explanation: S0189a is absent from Visser Table S1; its single holdout moves the global argmax to 0.0 s/deg, whereas the paired S0105a/S0189a holdout restores the canonical cell. The six-event single-removal results ship as Table 2. The non-agreement reported here is therefore not an artifact of the two-event selection difference. Event-exact declaration still matters, but at a finer grain: the archived published tables record S0325a at $\Delta = 39.7 \pm 6.1°$, inside the declared < 40° selection cut, while the Khan et al. (2023) distances used by Visser et al. list the same event at $40.8 \pm 1.7°$, outside it — the declared selection rule is catalog-dependent at its boundary, so the reproducible object is a declared, hash-pinned event list rather than a selection rule. Their materials are stated to be available on request; the present benchmark is public and runnable, so a cross-execution of the two pipelines on the exact declared event set is possible as soon as theirs is released.

6. Conclusions

Under the registered current public reconstruction of the Bi et al. (2025) PKiKP vespagram analysis: (i) a supported local maximum exists inside the published-pair target box (601.95 s, −6.67 s/deg) but ranks 6,938th in the lane, carrying 0.83× the power of (17% less than) a displaced, kinematically unexplained ridge 59.80 s after the published time at shallower slowness; (ii) across 24 evaluated surfaces — the full stack plus 23 one-at-a-time removals — six removals hand the ridge's rank-1 status to a time-adjacent shallow-slowness branch, not the target-box maximum, which never wins; multi-removal interactions were not tested; (iii) the registered alignment-jitter centroid and support statistics do not provide a feature-tracking exclusion test, while swapping the polarization operator relocates the envelope-A winner in time but leaves the target-box maximum non-global and the slowness mismatch unexplained; (iv) the peak-comparison table is byte-reproducible in the declared environment and root, while cross-root LOO replay preserves argmax semantics rather than NPZ container bytes; every claim-bearing number traces to a hash-pinned artifact; (v) registered same-data scramble calibration gives 75.5% ridge-power and 48.0% target-box-power exceedance rates under moveout-incoherent alternatives. Separately, non-attested exploratory injection lanes first out-compete the ridge at 0.25 in the processed-trace pre-P-RMS amplitude unit (§ 5.4); and (vi) a registered production pass of the authors' other deglitch method (`UCLA_v4`, run on raw data over the a-priori frozen executable 19-event sub-stack) leaves the qualitative disagreement and the subordination of the published-target maximum in place — the published-box maximum is cell-identical under both deglitch methods, while the global-argmax coordinate itself is deglitch-sensitive (§ 5.5). Single-station core-phase detections need — and with this benchmark, have — a public fragility instrument; a pre-registered lunar blind test of the same machinery shows why, producing "detections" in scrambled data and pure noise at false-alarm rates near one at exactly the uncertainty tightness the public reconstruction achieves (§ 5.3). The same-data scramble null closes that loop on the benchmark's own stack (§ 5.4).

Data and code availability

The complete pipeline, registered specification with amendment log, manifests, per-artifact SHA-256 identities, and all small claim-bearing tables are public in the reproducibility capsule at https://github.com/Percivio-Ltd/mars-inner-core-benchmark and archived as a versioned public deposit (DOI: 10.5281/zenodo.21762439); bulk stack products are hash-pinned in the capsule record and regenerable from public inputs. All input data are public (PDS/IRIS, MQS, IPGP Dataverse, Nature SI). Figures and tables are generated by `make_figures.py` from SHA-256-pinned recorded artifacts only; the generator asserts every annotated value against the recorded artifacts before writing output, and input/output digests are recorded in `figures/figure_provenance.json`.

Acknowledgements

This project used AI-assisted engineering and analysis (Anthropic Claude and OpenAI Codex model families) under registered human-controlled criteria; all scientific rules were frozen in versioned records before outcome inspection, and all claim-bearing numbers trace to hash-pinned artifacts (companion: NUMBERS.md). This work received no external funding.

Author contributions

Artus Krohn-Grimberghe (sole author), per the CRediT taxonomy: Conceptualization, Data curation, Formal analysis, Investigation, Methodology, Project administration, Resources, Software, Validation, Visualization, Writing – original draft, Writing – review & editing.

Competing interests

The author declares no competing interests.

References

- Beyreuther, M., Barsch, R., Krischer, L., Megies, T., Behr, Y., & Wassermann, J. (2010). ObsPy: A Python toolbox for seismology. *Seismological Research Letters*, 81(3), 530–533. https://doi.org/10.1785/gssrl.81.3.530
- Bi, H., Sun, D., Sun, N., Mao, Z., Dai, M., & Hemingway, D. (2025). Seismic detection of a 600-km solid inner core in Mars. *Nature*, 645, 67–72. https://doi.org/10.1038/s41586-025-09361-9 (Author Correction: *Nature*, 648, E18, 2025, https://doi.org/10.1038/s41586-025-09981-1; citation-only, not affecting the pick tables used here).
- Crotwell, H. P., Owens, T. J., & Ritsema, J. (1999). The TauP Toolkit: Flexible seismic travel-time and ray-path utilities. *Seismological Research Letters*, 70(2), 154–160. https://doi.org/10.1785/gssrl.70.2.154
- Garcia, R. F., Gagnepain-Beyneix, J., Chevrot, S., & Lognonné, P. (2011). Very preliminary reference Moon model. *Physics of the Earth and Planetary Interiors*, 188(1–2), 96–113. https://doi.org/10.1016/j.pepi.2011.06.015 (A 2012 erratum, https://doi.org/10.1016/j.pepi.2012.03.009, corrects a-priori deep moonquake locations and the internal pressure computation; its effect on the core-radius estimate cited here was not adjudicated here.)
- InSight Mars SEIS Data Service (2019). SEIS raw data, InSight Mission [data set]. IPGP, JPL, CNES, ETHZ, ICL, MPS, ISAE-Supaero, LPG, MSFC. https://doi.org/10.18715/SEIS.INSIGHT.

XB_2016 (accessed via PDS `urn:nasa:pds:insight_seis` v3.0 and FDSN network XB; exact input files SHA-256-pinned in `manifest/data_manifest.json`).

- InSight Marsquake Service (2023). Mars Seismic Catalogue, InSight Mission, V14 (2023-04-01) [data set]. ETHZ, IPGP, JPL, ICL, University of Bristol. https://doi.org/10.12686/a21
- Khan, A., Huang, D., Durán, C., Sossi, P., Giardini, D., & Murakami, M. (2023). Updated interior structure models of Mars with a liquid silicate layer atop the Martian core [data set]. IPGP Research Collection (Dataverse). https://doi.org/10.18715/IPGP.2023.llxn7e6d (deposit files incl. `Core.zip`, SHA-256-pinned in `manifest/data_manifest.json`).
- Lognonné, P., Banerdt, W. B., Giardini, D., Pike, W. T., Christensen, U., Laudet, P., de Raucourt, S., Zweifel, P., Calcutt, S., Bierwirth, M., Hurst, K. J., Ijpelaan, F., Umland, J. W., Llorca-Cejudo, R., Larson, S. A., Garcia, R. F., Kedar, S., Knapmeyer-Endrun, B., Mimoun, D., … Wookey, J. (2019). SEIS: InSight's seismic experiment for internal structure of Mars. *Space Science Reviews*, 215, 12. https://doi.org/10.1007/s11214-018-0574-6
- Montalbetti, J. F., & Kanasewich, E. R. (1970). Enhancement of teleseismic body phases with a polarization filter. *Geophysical Journal of the Royal Astronomical Society*, 21(2), 119–129. https://doi.org/10.1111/j.1365-246X.1970.tb01771.x
- Muirhead, K. J., & Datt, R. (1976). The N-th root process applied to seismic array data. *Geophysical Journal of the Royal Astronomical Society*, 47(1), 197–210. https://doi.org/10.1111/j.1365-246X.1976.tb01269.x
- Nunn, C., Garcia, R. F., Nakamura, Y., Marusiak, A. G., Kawamura, T., Sun, D., Margerin, L., Weber, R., Drilleau, M., Wieczorek, M. A., Khan, A., Rivoldini, A., Lognonné, P., & Zhu, P. (2020). Lunar seismology: A data and instrumentation review. *Space Science Reviews*, 216, 89. https://doi.org/10.1007/s11214-020-00709-3 (electronic supplement: Zenodo, https://doi.org/10.5281/zenodo.3560482).
- Apollo Passive Seismic Experiments (1969–1977). FDSN network XA [data set]. International Federation of Digital Seismograph Networks. https://doi.org/10.7914/SN/XA_1969

- Scholz, J.-R., Widmer-Schnidrig, R., Davis, P., Lognonné, P., Pinot, B., Garcia, R. F., Hurst, K., Pou, L., Nimmo, F., Barkaoui, S., de Raucourt, S., Knapmeyer-Endrun, B., Knapmeyer, M., Orhand-Mainsant, G., Compaire, N., Cuvier, A., Beucler, É., Bonnin, M., Joshi, R., … Banerdt, W. B. (2020). Detection, analysis, and removal of glitches from InSight's seismic data from Mars. *Earth and Space Science*, 7, e2020EA001317. https://doi.org/10.1029/2020EA001317
- Stähler, S., Khan, A., Banerdt, W. B., Lognonné, P., Giardini, D., Ceylan, S., Drilleau, M., Duran, A. C., Garcia, R. F., Huang, Q., Kim, D., Lekic, V., Samuel, H., Schimmel, M., Schmerr, N., Sollberger, D., Stutzmann, É., Xu, Z., Antonangeli, D., … Smrekar, S. E. (2021). Interior models of Mars from inversion of seismic body waves, V1.0 [data set]. IPGP Research Collection (Dataverse). https://doi.org/10.18715/IPGP.2021.kpmqrnz8
- Visser, M., Munch, F., Khan, A., Frost, D. A., & Giardini, D. (2026). No solid evidence for an inner core on Mars. Research Square preprint rs-10379955, version 1, posted 20 July 2026. https://doi.org/10.21203/rs.3.rs-10379955/v1 (preprint and supplement archived with SHA-256 provenance in this repository's reference library).
- Weber, R. C., Lin, P.-Y., Garnero, E. J., Williams, Q., & Lognonné, P. (2011). Seismic detection of the lunar core. *Science*, 331(6015), 309–312. https://doi.org/10.1126/science.1199375

Supplementary material: registered controls and their recorded outcomes

Supplement to "A registered public-data reproducibility benchmark for the reported PKiKP detection of a Martian inner core" (Krohn-Grimberghe). Table S1 sections S1a–S1f.

Each claim-bearing surface in this paper carries a positive control (a known-true value the implementation must reproduce) and an adverse or falsifying control (a deliberate corruption or null the implementation must reject). This table compacts the recorded outcomes; full identities, hashes, and run IDs are in the repository ledger and history records. Four entries deliberately document control weaknesses and their recorded dispositions — the fourth being the Earth pilot-gate failure and its post-hoc replacement (S1f) — and one records an adverse control whose firing blocked a confounded statistic (S1e) — reporting those is part of the benchmark's claim.

S1a — Input and provenance controls

Surface	Positive control (recorded outcome)	Adverse / falsifying control (recorded outcome)
Input integrity audit	2,393 versioned inputs checksum-valid (run `20260722T040215Z`)	Adverse manifest makes exactly the one intended file stale, nothing else
Deglitch lane status	26/26 events `succeeded_mps_only` in the accepted run	Strict `mps_ucla_verified` attestation FAILED and is reported as failed; the MPS-only lane is accepted by design, not silently upgraded
Rotation input gating	Audited input and isolated copy hash-identical; exact BHU/BHV/BHW at 20 Hz (S0105a)	Rotation fails closed when `deglitch_run_summary.json` is absent

S1b — Chain and peak-selection controls

Surface	Positive control (recorded outcome)	Adverse / falsifying control (recorded outcome)
End-to-end provenance chain	Accepted-run manifest: every stage succeeded, validation passed, current provenance requested and enforced	Peak detection with current-provenance enforcement exits blocked on a byte-flipped upstream trace
Peak-table reading (§ 4.1–4.2)	Figure layer re-derives the windowed supported argmax and target-box maximum and asserts equality with the recorded significance reading	A target box shifted by +100 s must not — and does not — reproduce the reading
Leave-one-out runner (§ 4.3)	Full-set restack reproduces the recorded cell exactly (663.80 s, −3.6364 s/deg, power 0.9327, support 23); S1015f hold-out repeat is byte-identical	Fail-closed tests: no supported in-window cell ⟹ nonzero exit, no artifacts. Documented weakness/ repair: the card's initial "full-grid" rule failed its own positive control (grid-edge artifact) and was repaired by a registered pre-execution amendment, not a silent patch

S1c — Resampling and operator controls

Surface	Positive control (recorded outcome)	Adverse / falsifying control (recorded outcome)
Composition association (§ 4.3)	Recorded branch fractions and Wilson CIs reproduced; synthetic composition label detected as material	Permuted-label lanes: Type I all null (p = 0.864/0.660/0.329); Type II 1 of 3 material — below the registered ≥ 2/3 void rule
PKKP occupancy concordance (§ 4.3)	All six recorded Type I/II argmax cells re-derived exactly from the pinned occupancy products	Documented weakness/ repair: the original transpose adverse control was vacuous by construction (recorded as such); replaced by a shape-preserving time-reversal control that reproduces 0/6 readings
Alignment-jitter audit (§ 4.4)	Zero-jitter lane reproduces base peak scalars to float32 identity; occupancy maps exactly binary	Audit power demonstrated: a 6×-excessive 60 s lane is material on both phases (PKiKP centroid displacement 27.9 s; PKKP 63.7 s) — the registered ±10 s lane's sensitivity is a finding, not an instrument floor
Polarization-operator ablation (§ 4.4)	80 operator-independent rows reproduce the benchmark exactly (max Δt = 0.000 s, max Δs = 0.000 s/deg); registered provenance-enforced rerun reproduces all 240 rows coordinate-identically with every row `current`	Zero rows carry the M-K operator label (lane-contamination check); in the enforced rerun a byte-flipped input trace fails closed as missing-current-provenance

S1d — Model and external-calibration controls

Surface	Positive control (recorded outcome)	Adverse / falsifying control (recorded outcome)
Reference-model kinematic query (§ 4.4)	P 224.131 s, PKiKP 808.136 s, differential 584.0 s — within 0.01 s of the registered criterion values	A 10° geometry shift moves the differential by > 5 s; an impossible query point matches zero rows
Lunar-analog blind test (§ 5.3; dated companion experiment)	Port fidelity: six of seven modules byte-identical to the audited Mars implementation (diff audit recorded); deterministic rerun byte-identical; catalogue and velocity-model checksums verified against live sources	Four-null suite is the experiment's central instrument: at replication grade, event-scramble fires 75/75, phase-randomized noise 72/75, station-swap 6/6, decoy windows 16/24 (FAR 0.67–1.00) while real paper-grade detections are 0/3. Custody: archived report + frozen PREREG (SHA `ab5f8034…`) + criteria code in git; bulk run products not retained

S1e — Same-data calibration controls (§ 5.4)

Surface	Positive control (recorded outcome)	Adverse / falsifying control (recorded outcome)
Event-scramble null (§ 5.4)	Identity permutation reproduces the canonical argmax and target-box cells with exact float equality on all seven recorded values, on grids array-identical to the canonical chain; regenerated lane line-identical to the production table (SHA `8df5f5c8…`)	Effect control: a single permutation changes 4,525,248 vespagram cells (max $\|\Delta\|$ 1357.7) — permuted distances cannot be silently ignored; seed-1 rerun byte-identical; sweep rows byte-identical to the control rows
Injection ladder (§ 5.4)	$\alpha = 0$ lane reproduces the canonical cell field-for-field under full provenance enforcement (240/240 rows current); production shift formula recovers the injected time 604.0 ± 0.051 s for 23/23 stacked traces in every lane; $\alpha = 1$ and $\alpha = 8$ reruns byte-identical including stack files	Documented weakness/ disposition: the $\alpha = 8$ literal "within one grid cell" control FAILED on the time axis (603.90 s = two 0.05-s cells from 604.0; slowness within one cell) and was adjudicated a control-tolerance design flaw — monotone α-convergence toward 604.0 from the in-box background maximum at 601.95 s; a convention error would displace by tens of seconds or flip sign. Not quotable as a passed literal control
Decoy-box family (§ 5.4)	Reader reproduces four independent recorded anchors exactly: canonical argmax cell; target-box maximum 0.7736; ridge-cell box 0.9327; pre-sweep-recorded PKKP threshold 0.2143	Frozen pre-P adverse box (required < 0.7736) returned 49.37 — the control FIRED and stopped the run, demonstrating the edge-ramp surface property; family fractions computed but confounded, not accepted; confirmatory family-rate lane on this surface closed

S1f — Earth known-truth control (§ 5.4)

Surface	Positive control (recorded outcome)	Adverse / falsifying control (recorded outcome)
Earth single-station port (§ 5.4)	Known-truth recovery expectation NOT met: PcP undetected at both frozen grades (PKiKP and ScS also undetected) ⟶ verdict NOT-RECOVERED at G1 and G2. Upstream, the registered pilot alignment gate FAILED (argmax +29.25 s at the search-window edge, envelope SNR 66×) and its statistic was replaced post hoc — an out-of-boundary deviation under the frozen repair rule; strict frozen reading: pilot FAIL ⟶ STOP, so the production run carries exploratory, deviation-flagged standing	Same-machinery nulls stayed quiet: FAR^PcP 0.000/0.080 (N1) and 0.000/0.250 (N2) at G1/G2 — all below the frozen 1/3 criterion, so the non-detection is not null-noise masking; at G2 the stack nonetheless certifies two wrong-place decoy windows. Full record, deviation log, and P2 backlog: `history/20260801_earth_ctrl/`